



## Reduction of the Structural Iron in Montmorillonite by Electron Transfer from Catechol and its Derivatives

Jasim Hamadi Hassen<sup>1\*</sup>  , Jack Silver<sup>2</sup> 

<sup>1</sup>University of Anbar, College of Pharmacy, Department of Pharmaceutical Chemistry, Ramadi, Iraq.

<sup>2</sup>University of Brunel, Wolfson Centre for Material Processing, London, UK.

**Abstract:** The structural Fe(III) in montmorillonite (MMT) clay has been reduced using catechol and its derivatives. It was found that the reduction process is pH-dependent and also depends on the ring substituents. If the catecholic ring has electron-donating substituents, reduction happens at high pH; if the catecholic ring has electron-withdrawing substituents, no reduction occurs. The process involves electron transfer from the hydroxy groups on the compounds to the active site at the iron atoms within the MMT lattice. This site acts as an electron acceptor (Lewis acid). Heat treatment of the reduced sample at 100-300 °C showed an enhancement of the Fe<sup>2+</sup>/Fe<sup>3+</sup> ratio, which is attributed to an increase in the proportion of radicalic formation induced by dehydration. The MMT sample was added to the solutions of the catecholic compound and the slurries were stirred for 24 hours in order to reach equilibrium, then filtered, washed, and air-dried. The reactions were monitored using Mössbauer spectroscopy, x-ray powder diffraction, differential thermal analysis, electron spin resonance, infrared, and total surface area determination.

**Keywords:** Catechol, montmorillonite, reduction, electron transfer.

**Submitted:** April 02, 2021. **Accepted:** October 11, 2021.

**Cite this:** Hassen JH, Silver J. Reduction of the Structural Iron in Montmorillonite by Electron Transfer from Catechol and its Derivatives. JOTCSA. 2021;8(4):1167-78.

**DOI:** <https://doi.org/10.18596/jotcsa.908713>.

**\*Corresponding author.** E-mail: [ph.jasimhu@uoanbar.edu.iq](mailto:ph.jasimhu@uoanbar.edu.iq), Tel: (009647805845839).

### INTRODUCTION

MMT belongs to the sizeable specific surface area clay minerals with a 2:1 layer structure. An octahedral sheet of alumina surrounded by two layers of tetrahedral silica sheets. There is an access net negative charge that can be balanced by cations like Na<sup>+</sup>, Ca<sup>2+</sup>, and Mg<sup>2+</sup> (1). The process of reducing structural iron of MMT and other clays has received significant interest from many researchers due to the wide application of this process in different fields. The iron existence in the clay mineral structure adds to its unique importance. The reason for this is the fact that the oxidation state can be changed and controlled by the influence of external factors. This in turn, leads to changes in the clay properties. The Fe oxidation state in the crystal lattice of MMT clay has an essential role in determining the surface and colloidal chemistry. It also plays an essential role

in the physical behavior of the clay. The valence states of clay's structural iron affect the physicochemical properties such as cation exchange capacity and surface area (2-4). Bacterial reduction of Fe-bearing clay has the ability to change the structure of the clay and causes a decrease in the surface area and an increase in the cation exchange capacity. The process is mainly reversible (5-7). A reduced nontronite clay has shown a noticeable antibacterial activity at pH 6 toward *E. coli* (8). It was found that *D. vulgaris* is able to reduce structural Fe(III) in four types of clay minerals (9). Humic acid can effectively stimulate the bioreduction rate of structural Fe(III) in clays (10). The Fe(II) in MMT was found to reduce 2-nitrophenol after adsorption (11). The reactivity of structural and surface-bonded Fe(II) in chemically reduced and oxidized nontronite and reduced MMT was investigated using two acetyl nitrobenzene



The mechanism of the MMT structural iron reduction by the catecholic compounds can be described as in Figure 3.

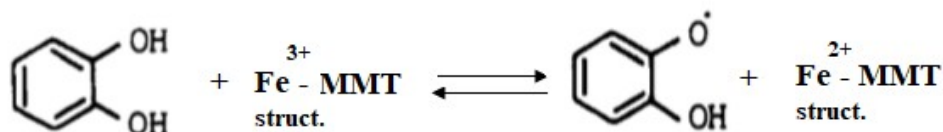


**Figure 3:** Mechanism of the MMT structural iron reduction by the catecholic compounds.

The radical produced in the last equation undergoes further oxidation to a quinone. For o-substituted compounds like catechol, the expected compound is o-benzoquinone (31).

### Mössbauer Spectroscopy

#### Mössbauer spectra of MMT-catechol

The Mössbauer spectra of the MMT sample reacted with catechol at pH 1 and 7 showed the same behavior as that of the original sample at the same pH; no effect was seen in the presence of catechol;

in fact, some of the iron(II) was oxidized to iron(III), presumably indirectly by oxygen contamination in the solution. The sample reacted with catechol at pH 10.5 shows a considerable enhancement of iron(II) at the expense of the iron(III) content. The  $\text{Fe}^{2+}/\text{Fe}^{3+}$  ratio derived from the Mössbauer spectrum was 2.4[5]. The parameter is presented in Table 1, and Figure 4 shows the spectra at 77 K of MMT sample reacted with catechol at pH 1, 7, and 10.5.

**Table 1:** The  $^{57}\text{Fe}$  Mössbauer parameters at 77 °K of the original MMT sample and the sample reacted with catechol at different pH's in an aqueous solution. Data were collected on the dried solids.

Sample	pH	$\delta$ mms <sup>-1</sup>	$\Delta$ mms <sup>-1</sup>	$\Gamma$ mms <sup>-1</sup>	Absorption area %	$\text{Fe}^{2+}/\text{Fe}^{3+}$ ratio
Original MMT	-	0.43[2]	0.65[2]	0.30[2]	51[4]	1[2]
		1.25[1]	3.03[1]	0.14[1]	49[3]	
MMT-catechol	1	0.43[1]	0.64[1]	0.31[1]	100	-
	7	0.39[1]	0.79[1]	0.40[2]	78[3]	0.3[1]
=	10.5	1.48[2]	2.56[4]	0.24[3]	22[4]	2.4[5]
		0.49[2]	0.73[4]	0.26[3]	30[5]	
		1.27[1]	3.04[1]	0.12[1]	70[4]	

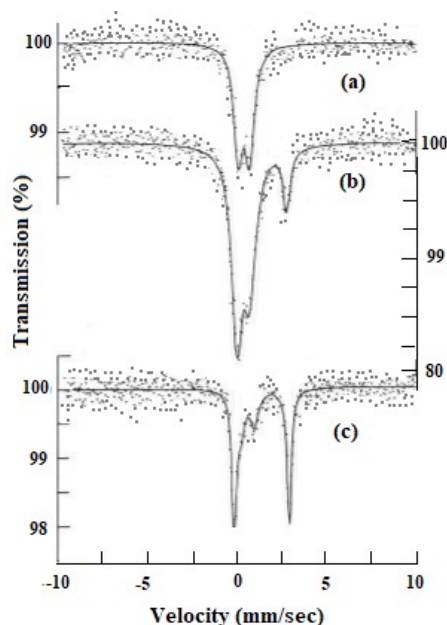


**Figure 4:** The  $^{57}\text{Fe}$  Mössbauer spectra at 77 °K of MMT reacted with catechol at (a) pH 1, (b) pH 7, (c) pH 10.5.

#### Mössbauer spectra of MMT-substituted catechol

Two substituted catechol compounds with electron-donating substituents, 4-tert-butylcatechol and 4-

methycatechol, and two compounds with electron-withdrawing substituents, 4-nitrocatechol and tetrabromocatechol were reacted with the MMT

sample at pH 10.5. The Mössbauer parameters are listed in Table 2, and the spectra of these samples are shown in Figure 5.

**Table 2:** The  $^{57}\text{Fe}$  Mössbauer parameters at 77 °K of the MMT samples reacted with different substituted catechol at pH 10.5 in an aqueous solution. Data were collected on the dried solids.

Samples	$\delta$ $\text{mms}^{-1}$	$\Delta$ $\text{mms}^{-1}$	$\Gamma$ $\text{mms}^{-1}$	Absorption area %	$\text{Fe}^{2+}/\text{Fe}^{3+}$ ratio
MMT-4-tert-butylcatechol	0.42[2]	0.74[2]	0.30[2]	30[3]	2.4[3]
	1.26[1]	3.04[1]	0.20[1]	70[2]	
MMT-4-methylcatechol	0.44[3]	0.76[3]	0.30[3]	29[4]	2.4[3]
	1.23[1]	3.02[1]	0.14[1]	71[3]	
MMT-4-nitrocatechol	0.44[1]	0.67[2]	0.28[2]	46[3]	1.2[2]
	1.26[1]	3.04[1]	0.16[1]	54[3]	
MMT-tetrabromocatechol	0.31[1]	0.82[3]	0.41[2]	78[6]	0.3[1]
	1.47[1]	2.60[2]	0.17[2]	22[3]	

The samples reacted with 4-tert-butylcatechol and 4-methylcatechol showed a clear reduction. While little or no reduction is observed in the sample reacted with 4-nitrocatechol and tetrabromocatechol compounds. The 4-nitro and tetrabromo are withdrawing substituents and tend to withdraw electron density from the catecholic

ring. The electron can be considered to reside on the substituent, leaving the molecule unable to transfer an electron to active sites on MMT. Electron-donating substituents, such as 4-tert-butyl and 4-methyl, facilitate electron transfer from the ring to the clay.

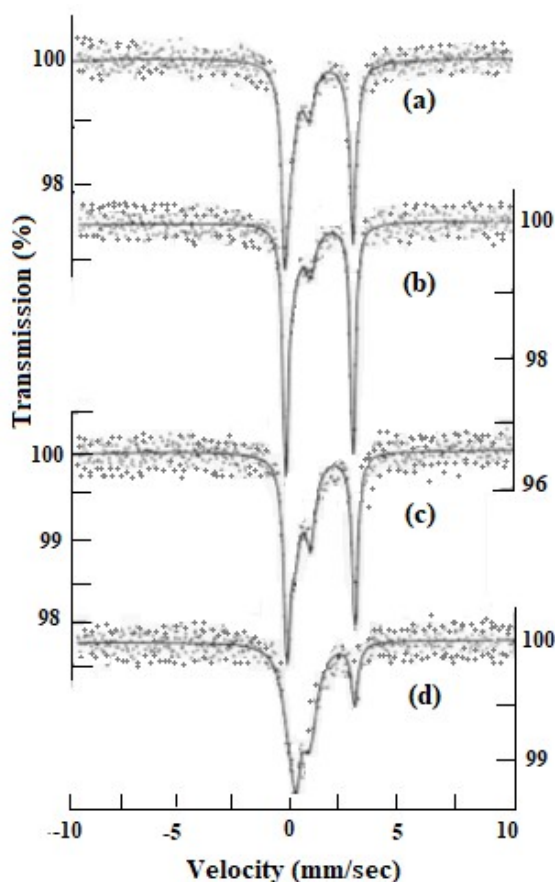


**Figure 5:** The  $^{57}\text{Fe}$  Mössbauer spectra at 77 °K of MMT reacted at pH 10.5 with (a) 4-tert-butylcatechol, (b) 4-methylcatechol, (c) 4-nitrocatechol, (d) tetrabromocatechol.

*Mössbauer spectra of the fired MMT-catechol sample*

In order to investigate the effect of firing on the powdered catechol-reduced MMT, the sample was subjected to a firing treatment ranging from 100 to

800 °C for a period of 10 minutes under air (Figure 6). As the firing temperature increased, the quadrupole splitting of the  $\text{Fe}^{3+}$  doublet shows a very small increase which indicates a mild distortion of the lattice. The linewidth of the  $\text{Fe}^{2+}$  peak became very narrow ( $\Gamma = 0.15 \text{ mms}^{-1}$ ), which indicates a unique type of coordination. Oxidation of the  $\text{Fe}^{2+}$  ions by firing occurred at higher temperatures than the original MMT sample. The  $\text{Fe}^{2+}$  doublet disappeared at 300 °C in the original sample, while its appearance continued to 600 °C in the MMT-catechol sample. The amount of  $\text{Fe}^{2+}$

increased with increasing the firing temperature from 100-300 °C and then decreasing with firing to a higher temperature as shown in the  $\text{Fe}^{2+}/\text{Fe}^{3+}$  ratio in Table 3. Other researchers noticed the reduction enhancement upon firing during the reaction between phenol and MMT (32). They attributed this to an enhancement of radical species induced by dehydration. The transferring of the electrons from the organic compounds to the active site of the  $\text{Fe}^{3+}$  may be facilitated by firing (Table 3).

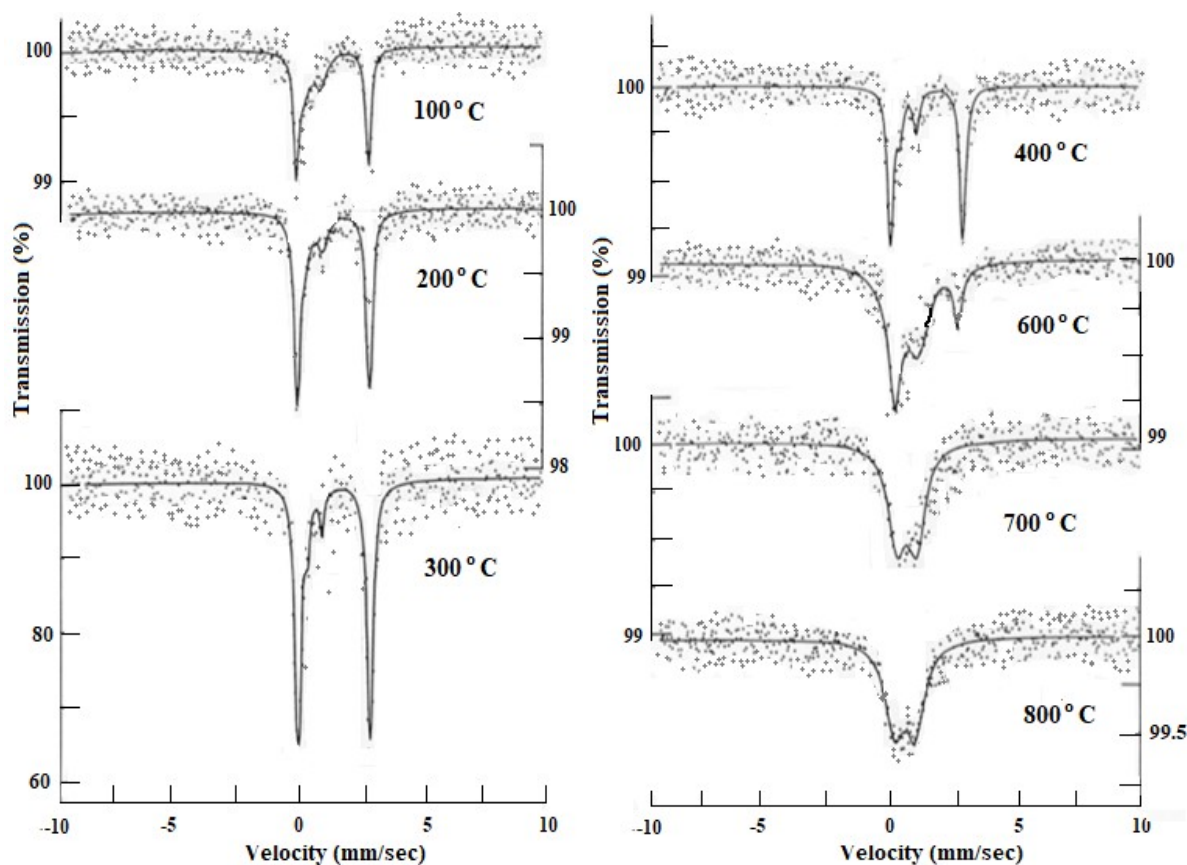


**Figure 6:** The  $^{57}\text{Fe}$  Mössbauer at 77 K of MMT-catechol samples reacted at pH 10.5 and fired in the air at various temperatures for 10 minutes. The temperature of firing is indicated.

**Table 3:** The  $^{57}\text{Fe}$  Mössbauer parameters at 77 K of the fired MMT-catecholic sample.

Temp.	$\delta \text{ mms}^{-1}$	$\Delta \text{ mms}^{-1}$	$\Gamma \text{ mms}^{-1}$	Absorption Area %	$\text{Fe}^{2+}/\text{Fe}^{3+}$ ratio
100 °C	0.43[4] 1.26[1]	0.65[5] 3.06[1]	0.31[5] 0.14[1]	39[8] 61[5]	1.6[4]
200 °C	0.44[3] 1.26[1]	0.73[5] 3.03[1]	0.27[4] 0.16[1]	24[5] 76[4]	3.3[9]
300 °C	0.46[4] 1.27[1]	0.57[6] 3.03[1]	0.12[5] 0.16[1]	11[7] 89[8]	14.3[9]
400 °C	0.48[1] 1.25[1]	0.67[5] 3.02[1]	0.15[4] 0.15[1]	22[8] 78[8]	4.2[1]
600 °C	0.41[3] 1.21[2]	0.96[5] 2.64[4]	0.53[5] 0.20[3]	21[7] 79[9]	4.3[1]
700 °C	0.36[2]	0.80[4]	0.44[4]	100	-
800 °C	0.31[2]	0.47[4]	0.47[4]	100	-

**X-Ray Powder Diffraction (XRD)**

The basal spacing of the air-dried MMT sample is 13 Å increasing to 17 Å on ethylene glycol treatment. When this sample heated at 120 °C for two hours, it showed partial collapse with a basal spacing of 12.62 Å. The collapse was completed on heating at 375 °C for 1 hour (Figure 7). MMT gives a basal spacing of 9.6 Å when no molecules are between the unit layers. The MMT sample that reacted with the catecholic compounds at pH 10.5 did not show the 13 Å basal spacing of the original sample, possibly due to the presence of sodium ions from the NaOH used to adjust the pH. The sample containing the organics did not show the 17 Å basal spacing on treatment with ethylene glycol again, which suggests that the ligands are present on the MMT crystal edges. These then cause blocking of some of the layers and prevent the complete swelling of ethylene glycol. In addition to this, the XRD pattern peaks obtained are slightly asymmetrical in the air-dried samples, which suggests a mixed-layer sequence (Table 4).

From the results listed in Table 4, there is no evidence for the intercalation of the catecholic compounds into the MMT interlayer. Therefore, an experiment was carried out to open the MMT lattice by dispersing 1 g of the MMT in a 50 mL solution of NaCl in water, as the sodium ions are able to open the interlayer to about 20 Å in water. The sample was allowed to stir for 1 hour, and then 100 mg of catechol was added, and the mixture was stirred for a further 24 hours. Upon examination, the sample showed no indications of

intercalation. The sample gave basal spacing of 12.3, 16.67, 12.45, and 11.78 Å for the air-dried, ethylene glycol treated, 120 °C heated, and 300 °C heated samples, respectively. At low pH, where no sodium ions are present, the basal spacing of the catechol-MMT sample was 13 Å, but the ethylene glycol treated sample did not swell to 17 Å, which provides further evidence for these compounds affecting the interlayer swelling. Figure 8 shows the XRD patterns of the air-dried MMT-catechol samples reacted at pH 1, 7, and 10.5.

**Differential Thermal Analysis, DTA**

DTA analysis showed that the curves of the original MMT sample subjected to pH's of 1, 7, and 10.5 are similar to the curve of the original sample. The change in pH does not affect the curve. When the MMT was reacted with the organic compounds, only the curves of the sample reacted at pH 10.5 were extensively modified (Figure 9). Catechol has two endothermic peaks at 100 and 200 °C (33), which do not appear on the curve of an MMT sample reacted with catechol, probably due to complexation with MMT. The main alteration in the curves of the sample reacted at pH 10.5 may be due to the formation of metal-ligand complexes adsorbed onto the clay surface since some cations such as iron are solubilized by catechol and expected to be found in the solution at high pH. Such complexes are associated with water molecules, which can be driven off as endothermic peaks before the first endothermic reaction of the MMT occurs.

**Table 4:** The basal spacing of some MMT-compounds.

Samples	----- d spacing in Å -----			
	Air-dried	EG	Heated at 120 °C 2 h.	Heated at 375 °C 1 h.
MMT	13	17	12.62	9.6
MMT-catechol pH 10.5	12.8	16.67	12.27	10.04
MMT-4-tert-butylcatechol pH 10.5	12.45	16.67	13.3	10.28
MMT-4-methylcatechol pH 10.5	12.27	16.67	12.81	9.71
MMT-4-nitrocatechol pH 10.5	12.27	16.67	13	9.71
MMT-tetrabromocatechol pH 10.5	11.94	16.67	13	9.71

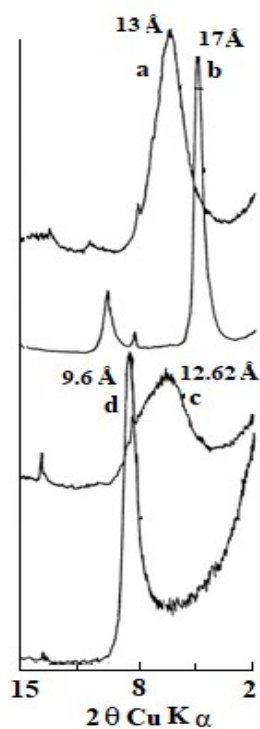


**Figure 7:** X-ray powder diffraction patterns of MMT (a) untreated sample, (b) treated with EG, (c) heated at 120 °C, (d) 375 °C.

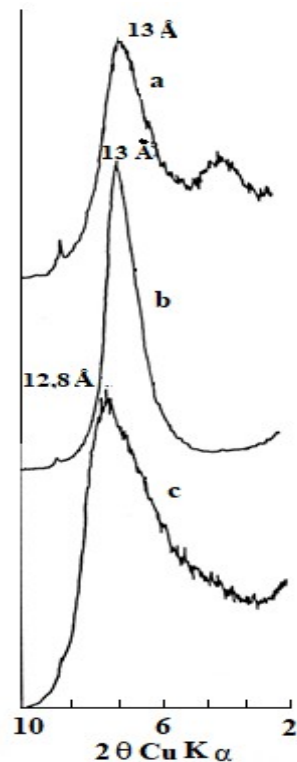


**Figure 8:** X-ray powder diffraction patterns of MMT-catechol sample reacted at (a) pH 1, (b) pH 7, (c) pH 10.5.

### Electron Spin Resonance (ESR)

Silicon, aluminum, magnesium and alkali, and alkaline earth metals are the most abundant ions usually found in clays that are diamagnetic. Paramagnetic ions such as  $\text{Fe}^{3+}$  may be found substituted for silicon, aluminum, or magnesium. The spectrum of the original sample is characterized by features with g-values of 2.0, 2.2, 3.7, 4.3, and 9.6, similar to the result reported by other workers (34). The ESR features with g-values of 3.7, 4.3, and 9.6 have been assigned to  $\text{Fe}^{3+}$  in a site of near rhombic symmetry, while the other features arise from  $\text{Fe}^{3+}$  in a different type of environment (Figure 10).

The sample of catechol-reduced MMT exhibits substantial changes in the main features of the spectra. The 2.2 and 9.6 g-value signals are broader than those found in the untreated sample. The 3.7 g-value signals disappeared from the spectra, and that with a g-value of 4.3 was narrower and less intense than in the untreated sample. The reduction of MMT with catechol caused a reduction in the intensities of the signals, which can be assigned to the structural  $\text{Fe}^{3+}$ . This result

is in good agreement with the Mössbauer data, which revealed an incomplete reduction of the structural  $\text{Fe}^{3+}$ . An enhancement in the  $g = 2.0$  signal was observed due to the formation of a radical. This signal is similar to those reported by other workers (35) obtained from the reaction of some aromatic molecules with clays. The reaction of the hydroxybenzene compounds with the MMT involves a radical formation in the first stage, which oxidized to a quinone at a later stage. From the ESR results, it appears that part of these compounds remains in the radical (semiquinone) form on the MMT surface. These radicals are responsible for the signal at  $g = 2.0$ .

Similar behavior in the ESR spectra was observed for the MMT samples reduced by 4-methyl and 4-tert-butylcatechol, which have electron-donating ability (Figure 10). The  $g = 2.0$  signal was greatly enhanced in the sample reduced with 4-tert-butylcatechol. However, there were some remnants of the signal at  $g = 3.7$ . Reaction with the 4-nitro and tetrabromo substituents also showed an enhancement of the signal  $g = 2.0$ , and the  $g = 2.2$  signal became broader.

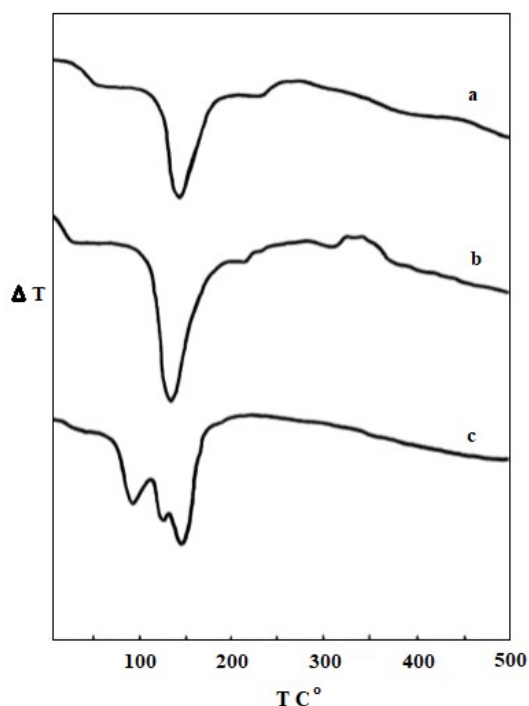


**Figure 9:** DTA curves of MMT reacted with catechol at (a) pH 1, (b) pH 7, (c) pH 10.5.

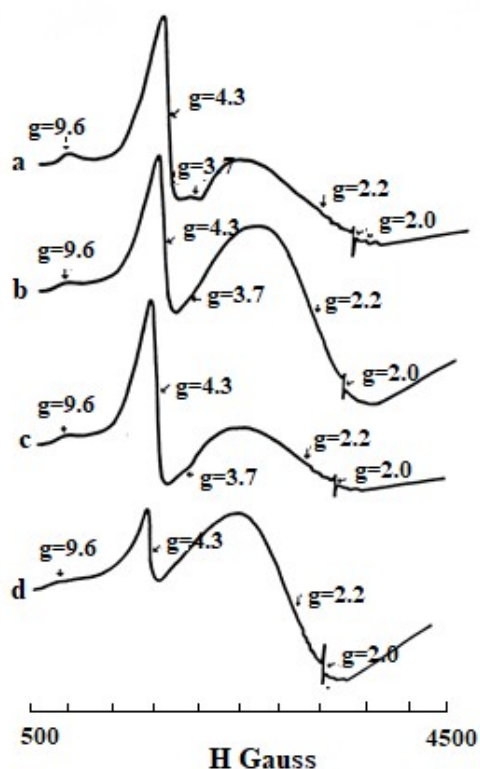


**Figure 10:** ESR spectra at room temperature of (a) MMT, MMT reacted with catechol at (b) pH 1, (c) pH 7, (d) pH 10.5.

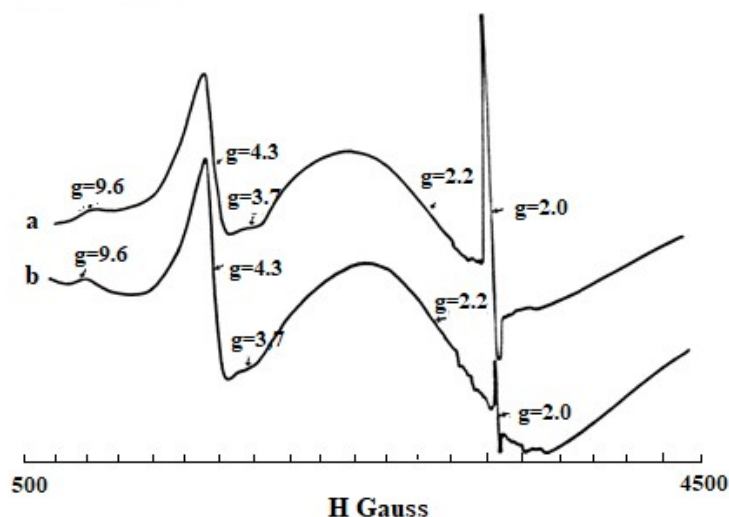


**Figure 10:** ESR spectra at room temperature of MMT reacted at pH 10.5 with (a) 4-tert-butylcatechol, (b) 4-methylcatechol.

### Infra-Red Spectra (IR)

The MMT's main features in the IR region are the Si-O stretching and OH bending. The position of these bands are at 800, 850, 880, 917, and 1040  $\text{cm}^{-1}$  and are assigned to  $\text{Fe}^{3+}\text{-OH-Fe}^{3+}$ ,  $\text{Al-OH-Mg}$ ,  $\text{Fe}^{3+}\text{-OH-Al}$ ,  $\text{Al-OH-Al}$ , and  $\text{Si-O}$ , respectively (36,37) (Table 5). The IR spectrum also exhibits bands due to the adsorbed compounds on the MMT, but we will discuss only the effect of these compounds on the prominent montmorillonite

bands. The sharpness and position of OH bending modes of the sample reacted with different compounds varies from one compound to another.

The Si-O stretching band at 1040  $\text{cm}^{-1}$  and the  $\text{Fe}^{3+}\text{-OH-Al}$  band at 880  $\text{cm}^{-1}$  disappeared in most of the samples. The disappearance of the latter band is noticeable in the reduced samples. This band disappeared in MMT and nontronite samples reduced with hydrazine and dithionite, and its

disappearance was attributed to the protonation of the adjacent OH group (30). The band at  $800\text{ cm}^{-1}$  in the catechol reduced MMT sample, which is assigned to  $\text{Fe}^{3+}\text{-OH-Fe}^{3+}$  bending, is shifted to  $790\text{ cm}^{-1}$ . This shift has also been found in some other samples. The band at  $850\text{ cm}^{-1}$ , which is assigned to Al-OH-Mg bending, is shifted to  $838\text{ cm}^{-1}$ . Both bands are enhanced upon reduction with catechol. The  $880\text{ cm}^{-1}$  band disappeared from the catechol reduced sample and also from the substituted catechol reduced samples, 4-methyl and 4-tert-butyl catechol.

### Total Surface Area Determination

The total surface area is a fundamental property of clays. It can be determined by the retention of ethylene glycol (EG). MMT clay can take two layers of EG molecules between the interlayer spacing. The resultant areas were calculated using Dyal and Hendricks (38) value of  $810\text{ m}^2/\text{g}$  for the total surface area of MMT. The original MMT sample gave a value of  $839\text{ m}^2/\text{g}$  (Table 6). This value was decreased by about  $100\text{ m}^2/\text{g}$  in the sample reacted with the compounds at pH 10.5, which is attributed to the presence of these compounds on the crystal edges of MMT causes blocking of some

layers, preventing complete swelling. No apparent decrease in the values was found in the sample reacted at pH 1 and 7. The possibility of the presence of the organic compounds on the crystal edges at pH 10.5 seems greater than at pH 1 and 7. This may be due to the formation of complexes of these compounds and cations that are liberated at high pH. These complexes increase the possibility of blocking the layers.

### CONCLUSIONS

Catecholic compounds containing electron-donating substituents have the ability to reduce the structural iron of MMT at high pH. The process depends on the pH, ring substituents and conjugation. No reduction occurs if the catecholic ring has electron-withdrawing substituents. The process involves electron transfer from the hydroxy groups on the compounds to the active site at the iron atoms within the MMT lattice. The reduction process can be enhanced by heating the powdered sample up to  $300\text{ }^\circ\text{C}$ . The  $\text{Fe}^{2+}/\text{Fe}^{3+}$  ratio increases due to the increase in the proportion of radical formation induced by dehydration.

**Table 5:** Selected features of the infra-red spectra ( $\text{cm}^{-1}$ ) of the MMT sample reacted with the catecholic compounds.

Sample	pH	Si-O	Al-OH-Al	$\text{Fe}^{3+}\text{-OH-Al}$	Al-OH-Mg	$\text{Fe}^{3+}\text{-OH-Fe}^{3+}$
MMT	-	1050 sh	917 w	880 w	850 m	800 s
MMT-catechol	10.5	-	915 sh	-	838 s	790 s
MMT-4-nitrocatechol	=	-	915 w	890 sh	848 m	800 m
MMT-tetrabromocatechol	=	1015 sh	918 w	885 sh	835 m	795 s
MMT-4-methylcatechol	=	-	915 m	-	845 m	800 m
MMT-4-tert-butylcatechol	=	-	913 s	-	840 m	795 s

**Table 6:** The total surface areas of the samples.

Samples	pH	Total surface area in $\text{m}^2/\text{g}$
MMT	-	839
MMT-catechol	10.5	710
MMT-4-methylcatechol	10.5	629
MMT-4-tert-butylcatechol	10.5	634
MMT-4-nitrocatechol	10.5	641
MMT-tetrabromocatechol	10.5	622

### REFERENCES

1. Ziemiański P, Kałahurska K, Samojedan B. Selective catalytic reduction of NO with  $\text{NH}_3$  on mixed alumina-iron (III) oxide pillared

montmorillonite "Cheto" Arizona, modified with hexamminecobalt (III) chloride. Adsorption Science & Technology. 2017 Dec;35(9-10):825-33. <DOI>.

2. Pentráková L, Su K, Pentrák M, Stucki JW. A review of microbial redox interactions with structural Fe in clay minerals. *Clay miner.* 2013 Jun;48(3):543–60. [<DOI>](#).
3. Luan F, Liu Y, Griffin AM, Gorski CA, Burgos WD. Iron(III)-Bearing Clay Minerals Enhance Bioreduction of Nitrobenzene by *Shewanella putrefaciens* CN32. *Environ Sci Technol.* 2015 Feb 3;49(3):1418–26. [<DOI>](#).
4. Lee K, Kostka JE, Stucki JW. Comparisons of structural Fe reduction in smectites by bacteria and dithionite: an infrared spectroscopic study. *Clays Clay Miner.* 2006 Apr 1;54(2):195–208. [<DOI>](#).
5. Perdril JN, Warr LN, Perdril N, Lett M-C, Elsass F. Interaction between smectite and bacteria: Implications for bentonite as backfill material in the disposal of nuclear waste. *Chemical Geology.* 2009 Jun;264(1–4):281–94. [<DOI>](#).
6. Stucki JW, Kostka JE. Microbial reduction of iron in smectite. *Comptes Rendus Geoscience.* 2006 Jun;338(6–7):468–75. [<DOI>](#).
7. Pentráková L, Su K, Pentrák M, Stucki JW. A review of microbial redox interactions with structural Fe in clay minerals. *Clay miner.* 2013 Jun;48(3):543–60. [<DOI>](#).
8. Wang X, Dong H, Zeng Q, Xia Q, Zhang L, Zhou Z. Reduced Iron-Containing Clay Minerals as Antibacterial Agents. *Environ Sci Technol.* 2017 Jul 5;51(13):7639–47. [<DOI>](#).
9. Liu D, Dong H, Bishop ME, Zhang J, Wang H, Xie S, et al. Microbial reduction of structural iron in interstratified illite-smectite minerals by a sulfate-reducing bacterium: Bioreduction of structural iron in clay minerals by a SRB. *Geobiology.* 2012 Mar;10(2):150–62. [<DOI>](#).
10. Liu G, Qiu S, Liu B, Pu Y, Gao Z, Wang J, et al. Microbial reduction of Fe(III)-bearing clay minerals in the presence of humic acids. *Sci Rep.* 2017 Jun;7(1):45354. [<DOI>](#).
11. Wu H, Song Z, Lv M, Zhao D, He G. Iron-Pillared Montmorillonite As An Inexpensive Catalyst For 2-Nitrophenol Reduction. *Clays Clay Miner.* 2018 Oct;66(5):415–25. [<DOI>](#).
12. Hofstetter TB, Neumann A, Schwarzenbach RP. Reduction of Nitroaromatic Compounds by Fe(II) Species Associated with Iron-Rich Smectites. *Environ Sci Technol.* 2006 Jan 1;40(1):235–42. [<DOI>](#).
13. Sugiura Y, Tomura T, Ishidera T, Doi R, Francisco PCM, Shiwaku H, et al. Sorption behavior of selenide on montmorillonite. *J Radioanal Nucl Chem.* 2020 May;324(2):615–22. [<DOI>](#).
14. Latta DE, Neumann A, Premaratne WAPJ, Scherer MM. Fe(II)–Fe(III) Electron Transfer in a Clay Mineral with Low Fe Content. *ACS Earth Space Chem.* 2017 Jun 15;1(4):197–208. [<DOI>](#).
15. Zeng Q, Dong H, Wang X. Effect of ligands on the production of oxidants from oxygenation of reduced Fe-bearing clay mineral nontronite. *Geochimica et Cosmochimica Acta.* 2019 Apr;251:136–56. [<DOI>](#).
16. Notini L, Latta DE, Neumann A, Pearce CI, Sassi M, N'Diaye AT, et al. A Closer Look at Fe(II) Passivation of Goethite. *ACS Earth Space Chem.* 2019 Dec 19;3(12):2717–25. [<DOI>](#).
17. Notini L, Latta DE, Neumann A, Pearce CI, Sassi M, N'Diaye AT, et al. The Role of Defects in Fe(II)–Goethite Electron Transfer. *Environ Sci Technol.* 2018 Mar 6;52(5):2751–9. [<DOI>](#).
18. Joe-Wong C, Brown GE, Maher K. Kinetics and Products of Chromium(VI) Reduction by Iron(II/III)-Bearing Clay Minerals. *Environ Sci Technol.* 2017 Sep 5;51(17):9817–25. [<DOI>](#).
19. Liu X, Dong H, Zeng Q, Yang X, Zhang D. Synergistic Effects of Reduced Nontronite and Organic Ligands on Cr(VI) Reduction. *Environ Sci Technol.* 2019 Dec 3;53(23):13732–41. [<DOI>](#).
20. Liao W, Ye Z, Yuan S, Cai Q, Tong M, Qian A, et al. Effect of Coexisting Fe(III) (oxyhydr)oxides on Cr(VI) Reduction by Fe(II)-Bearing Clay Minerals. *Environ Sci Technol.* 2019 Dec 3;53(23):13767–75. [<DOI>](#).
21. Joe-Wong C, Weaver KL, Brown ST, Maher K. Chromium isotope fractionation during reduction of Chromium(VI) by Iron(II/III)-bearing clay minerals. *Geochimica et Cosmochimica Acta.* 2021 Jan;292:235–53. [<DOI>](#).
22. Carriazo J, Guérou E, Barrault J, Tatibouët JM, Molina R, Moreno S. Catalytic wet peroxide oxidation of phenol by pillared clays containing Al–Ce–Fe. *Water Research.* 2005 Oct;39(16):3891–9. [<DOI>](#).
23. Cheng J, Ming Yu S, Zuo P. Horseradish peroxidase immobilized on aluminum-pillared interlayered clay for the catalytic oxidation of phenolic wastewater. *Water Research.* 2006 Jan;40(2):283–90. [<DOI>](#).
24. Ko CH, Fan C, Chiang PN, Wang MK, Lin KC. p-Nitrophenol, phenol and aniline sorption by organo-clays. *Journal of Hazardous Materials.* 2007 Oct;149(2):275–82. [<DOI>](#).

25. Shakir K, Ghoneimy HF, Elkafrawy AF, Beheir ShG, Refaat M. Removal of catechol from aqueous solutions by adsorption onto organophilic-bentonite. *Journal of Hazardous Materials*. 2008 Feb;150(3):765–73. [<DOI>](#).
26. Liu Y, Gao M, Gu Z, Luo Z, Ye Y, Lu L. Comparison between the removal of phenol and catechol by modified montmorillonite with two novel hydroxyl-containing Gemini surfactants. *Journal of Hazardous Materials*. 2014 Feb;267:71–80. [<DOI>](#).
27. Hassen JH. Montmorillonite Nanoclay Interaction with 2-Aminophenol and 2-Nitrophenol. *Rese Jour of Pharm and Technol*. 2019;12(6):2828. [<DOI>](#).
28. Eltantawy IM, Arnold PW. Reappraisal Of Ethylene Glycol Mono-Ethyl Ether (Egme) Method For Surface Area Estimations Of Clays. *Journal of Soil Science*. 1973 Jun;24(2):232–8. [<DOI>](#).
29. Solomon DH, Loft BC, Swift JD. Reactions catalysed by minerals. IV. The mechanism of the benzidine blue reaction on silicate minerals. *Clay miner*. 1968 Dec;7(4):389–97.
30. Rozenson I. Reduction and Oxidation of Fe<sup>3+</sup> in Dioctahedral Smectites—1: Reduction with Hydrazine and Dithionite. *Clays and Clay Minerals*. 1976;24(6):271–82. [<DOI>](#).
31. Sofen SR, Ware DC, Cooper SR, Raymond KN. Structural, electrochemical, and magnetic properties of a four-membered redox series ([Cr(L3)]<sub>n</sub>-, n = 0-3) in catechol-benzoquinone complexes of chromium. *Inorg Chem*. 1979 Feb 1;18(2):234–9. [<DOI>](#).
32. Isaacson PJ, Sawhney BL. Sorption and transformation of phenols on clay surfaces: effect of exchangeable cations. *Clay miner*. 1983 Sep;18(3):253–65. [<DOI>](#).
33. Greene-Kelly R. The Montmorillonite Minerals (Smectites). In: Mackenzie R, editor. *The Differential Thermal Investigation of Clay*. London: Mineralogical Society; 1957. p. 140–64.
34. Goodman BA. An investigation by Mössbauer and EPR spectroscopy of the possible presence of iron-rich impurity phases in some montmorillonites. *Clay miner*. 1978 Sep;13(3):351–6. [<DOI>](#).
35. Pinnavaia TJ, Hall PL, Cady SS, Mortland MM. Aromatic radical cation formation on the intracrystal surfaces of transition metal layer lattice silicates. *J Phys Chem*. 1974 May;78(10):994–9. [<DOI>](#).
36. Rozenson I. Reduction and Oxidation of Fe<sup>3+</sup> in Dioctahedral Smectites—III.\* Oxidation of Octahedral Iron in Montmorillonite. *Clays and Clay Minerals*. 1978;26(2):88–92. [<DOI>](#).
37. Holtzer M, Bobrowski A, Grabowska B. Montmorillonite: a comparison of methods for its determination in foundry bentonites. *Metalurgija*. 2011;50(2):119–22.
38. Dyal RS, Hendricks SB. Total surface of clays in polar liquids as a characteristic index: soil science. 1950 Jun;69(6):503–9. [<DOI>](#).

